Crop Protection 109 (2018) 42–50

Contents lists available at ScienceDirect

Crop Protection

journal homepage: www.elsevier.com/locate/cropro

Proximal hyperspectral sensing of stomatal conductance to monitor the efficacy of exogenous abscisic acid applications in apple trees

Sanaz Jarolmasjed[a], Sindhuja Sankaran[a,c,*], Lee Kalcsits[b], Lav R. Khot[a,c]

[a] Department of Biological Systems Engineering, Washington State University, Pullman, WA, United States
[b] Tree Fruit Research and Extension Center, Washington State University, Wenatchee, WA, United States
[c] Center for Precision and Automated Agricultural Systems, Washington State University, Prosser, WA, United States

ARTICLE INFO

Keywords:
Partial least square regression
Support vector machine
Feature selection
Visible near-infrared spectral reflectance

ABSTRACT

Stomatal conductance is a critical regulating factor in plant water relations and responses to abiotic stress. Abscisic acid (ABA) is one of the plant hormones that regulates stomatal conductance and leaf transpiration. The presence of endogenous or exogenous ABA induces stomatal closure, which reduces leaf transpiration rates and increases tolerance to abiotic stress. In this study, visible near-infrared (Vis-NIR) spectroscopy, as well as proximal multispectral and thermal imaging were used to evaluate changes in stomatal conductance through exogenous ABA applications to apple trees. ABA was applied twice at 500 mg kg^{-1} in 2016, with five control and five ABA-treated trees in a three-year-old apple orchard. Proximal Vis-NIR spectral reflectance (350–2500 nm) data, and multispectral and thermal infrared images were acquired from control and treated trees after 1–3 days of exogenous ABA application to the trees. Ground reference stomatal conductance was also measured to compare the data with proximal sensing data. Partial least square regression (PLSR), linear support vector machines (SVM), and quadratic SVM algorithms were applied to classify the control and ABA-treated leaves, before and after feature selection using rank features technique and stepwise regression analysis. The average classification accuracy ranged between 80 and 85% at 3 days after treatment with the entire Vis-NIR spectra, while the accuracies ranged between 74 and 80% with five selected spectral bands. The ABA treatment effects could not be observed with crop water stress index extracted from thermal images, although the leaf temperature in ABA-treated trees were higher than the untreated control trees. Green normalized difference vegetation index extracted from multispectral images also did not show any differences between control and ABA-treated trees. Overall, results suggest that the hyperspectral Vis-NIR sensing was able to acquire spectral changes pertinent to the dynamic processes such as stomatal conductance, independent from non-responsive traditional vegetation indices that lacked responsive spectral bands.

1. Introduction

The measurement of plant water status is important to improve upon the ability to optimize irrigation decisions. Improving water-use efficiency can have ecological as well as horticultural benefits. Changes in plant water status can affect tree growth, physiology, productivity and crop quality (Espinoza et al., 2017). The dynamic management of plant water in horticultural crops can be a valuable tool to improve growth, productivity, and quality (Shackel et al., 1997). The success of above strategy depends on the ability to rapidly and accurately measure changes in plant water status to make informed irrigation decisions. In many crops, stomatal conductance has been shown to be closely linked to plant water status. Traditional measures of stomatal conductance have been focused on measuring water loss from a defined leaf area surface. However, emerging strategies are focused on rapid, proximal sensing to detect changes in plant water status (Espinoza et al., 2017). Proximal sensing of leaf stomatal conductance has implications that extend beyond irrigation management and is important for maintaining optimum plant health.

Abscisic acid (ABA) is a growth regulator that is produced in both the roots and shoots and is translocated to other parts of the plant through xylem during the transpiration process (Coggins and Lovatt, 2014). ABA manages plant responses to water stress by coordinating stomatal conductance with the available water supply (Aasamaa and Sõber, 2011). ABA regulates stomatal closure (Correia et al., 1995), leaf transpiration, and plant water potential (Freitas et al., 2011). Under water stress conditions, ABA induces stomatal closure to conserve water (García-Mata and Lamattina, 2003) and to reduce the risk of damage to

* Corresponding author. Department of Biological Systems Engineering, Washington State University, Pullman, WA, United States.
E-mail address: sindhuja.sankaran@wsu.edu (S. Sankaran).

https://doi.org/10.1016/j.cropro.2018.02.022
Received 28 November 2017; Received in revised form 19 February 2018; Accepted 23 February 2018
Available online 20 March 2018
0261-2194/ Published by Elsevier Ltd.

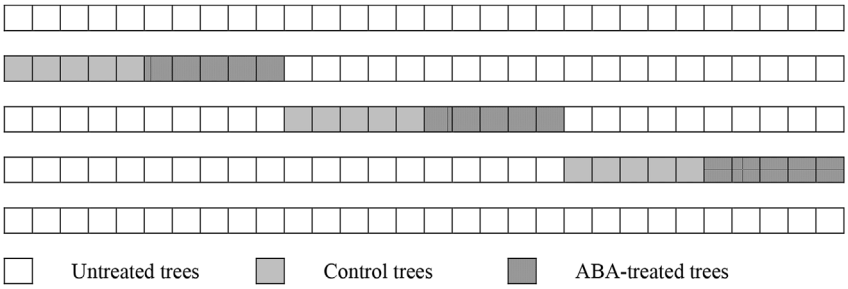

Fig. 1. Plot design describing the treatments in the Sunrise orchard.

the plant. ABA accumulates in shoots that reduces leaf transpiration without significantly affecting the fruit transpiration (Freitas et al., 2011).

Plant water use efficiency is influenced by water uptake and transport wherein leaf transpiration plays a major role. Exogenous or synthetic ABA can also be used to induce drought stress responses in the absence of stress conditions (Shinozaki and Yamaguchi-Shinozaki, 2007). McArtney et al. (2014) reported that exogenous synthetic ABA applications to apple canopy induces stomatal closure and decreases stomatal conductance. There is growing interest in being able to monitor the effect of exogenous ABA applications on stomatal conductance and plant water status. ABA can limit transplant shock (Berkowitz and Rabin, 1988), induce dormancy (Hilhorst and Karssen, 1992), increase fruit quality (Kobashi et al., 1999), and has been reported to induce greater fruit calcium accumulations in tomato (Freitas et al., 2011).

Fruit calcium absorption is important in preventing some physiological disorders in fleshy horticultural crops (Ho and White, 2005). Calcium is absorbed from the soil through root water uptake. Xylem water movement is required for calcium uptake and delivery to sink organs such as leaves and fruit. The difference in transpiration rates between leaves and fruit has been hypothesized as a mechanism that leads to calcium imbalances between these two competing organs. When ABA production is induced in the plant by water stress or when exogenous ABA is applied, stomata closure leads to declined transpiration rate. This may influence the transpirational balance between fruit and leaves and produce an increase in calcium uptake in developing fruit. Freitas et al. (2011) reported that calcium uptake and distribution into the developing tomato fruit was greater when exogenous ABA was applied because of reductions in leaf transpiration. Exogenous ABA increased calcium uptake into the fruit and reduced blossom end rot in tomato (Freitas et al., 2011). Similar experiments in apricot (Montanaro et al., 2010) and kiwi (Montanaro et al., 2012) have demonstrated a close association between transpiration and calcium accumulation. In apple, ABA has been reported to affect calcium-related genes (Falchi et al., 2017) and to reduce transpiration that can have a strong effect on calcium levels in the fruit. Although the effect of ABA on plant physiology has been well documented, practical limits on the real-time monitoring of plant responses to ABA are difficult and time consuming to measure. As such, there needs to be better monitoring method developed for the use of exogenous ABA treatments.

The effect of ABA on leaf and plant physiology can be estimated through the direct measure of evapotranspiration, photosynthetic rate, and stomatal conductance (Astacio and Iersel, 2011). Advanced high-throughput plant sensing tools to accurately monitor the effect of ABA on plants/trees are essential in optimizing exogenous ABA applications. Proximal and remote sensing techniques such as visible near-infrared (Vis-NIR) spectroscopy and imaging have been used to evaluate biotic stress status (Calderón et al., 2013; Gomez-Candon et al., 2014; Naidu et al., 2009; Sankaran et al., 2011). High-throughput vegetation temperature measurement can also serve as an indicator of transpiration rate and stomatal conductance changes (Berni et al., 2009; Calderón et al., 2014; Zarco-Tejada et al., 2012). Stomata closure results in lower transpiration rate that increases the leaf temperature (Osakabe et al., 2014). Thus, thermal imaging may be useful in estimating the plant water use efficiency, and consequently abiotic and biotic stress in plants (Araus and Cairns, 2014; Chaerle et al., 2005). For example, the spatial variability of water stress in a vineyard has been assessed with extracted crop water stress index (CWSI) using temperature data (Bellvert et al., 2014). The CWSI was found to be highly correlated with leaf water potential (coefficient of determination, $R^2 = 0.83$).

Currently, stomatal conductance is monitored using handheld or stationary instrumentation that monitors shifts in relative humidity gradients, which can be used to estimate plant transpiration, a measure of stomatal conductance. In this study, we hypothesize that decreases in stomatal conductance induced by exogenous ABA applications to apple trees can be monitored using proximal visible-near infrared and thermal sensing systems. The objectives were to evaluate the response of the apple trees to exogenous ABA application using proximal visible near-infrared spectroscopy, and agricultural utility vehicle (AUV)-based thermal infrared and multispectral imaging with controlled experimentation and provide comparisons of such data with direct physiological measurements.

2. Materials and methods

2.1. Field site, experimental design, and ABA treatments

The experiment was conducted at Washington State University's Sunrise Research Orchard located in Rock Island, WA (47°18′35.27″N, 120° 4′0.16″W). The 'Honeycrisp' apple orchard on M9-T337 rootstock was planted in 2015 and did not contain fruit at the time of measurements. Three replicates of 10 trees were selected for uniformity and health from the four rows of 60 trees in a split-plot experimental design. Each replicate was split into two groups of five trees; one to act as an untreated control and the other for ABA to be applied (Fig. 1). ABA was applied at a rate of 500 mg kg^{-1} to the point of drip formation on the leaves using a backpack sprayer on two dates; June 20 and August 16, 2016. ABA has been shown to be biologically active for approximately 21 days in young apple trees (McArtney et al., 2014) and the time between treatments was chosen to exceed that period.

2.2. Ground reference measurements

Stomatal conductance was measured immediately prior to sensor-based measurements in the same location. Measurements were made using a Decagon SC-15 handheld porometer (Meter Group Inc., WA, USA) between 09:00 and 11:00 a.m. on sunny days when the photosynthetically active radiation was between 1200 and 1500 μmol m^{-2} s^{-1} on two sun-exposed leaves that were approximately 1.5 m from the ground. The porometer used in this study considers the air relative humidity and temperature in the calibration process. For leaf measurement, the sensor obtains leaf humidity and estimates the stomatal conductance according to the difference between relative humidity in two conductance elements inside the sensor. Air temperature during measurements was between 18 and 20 °C (AgWeatherNet at

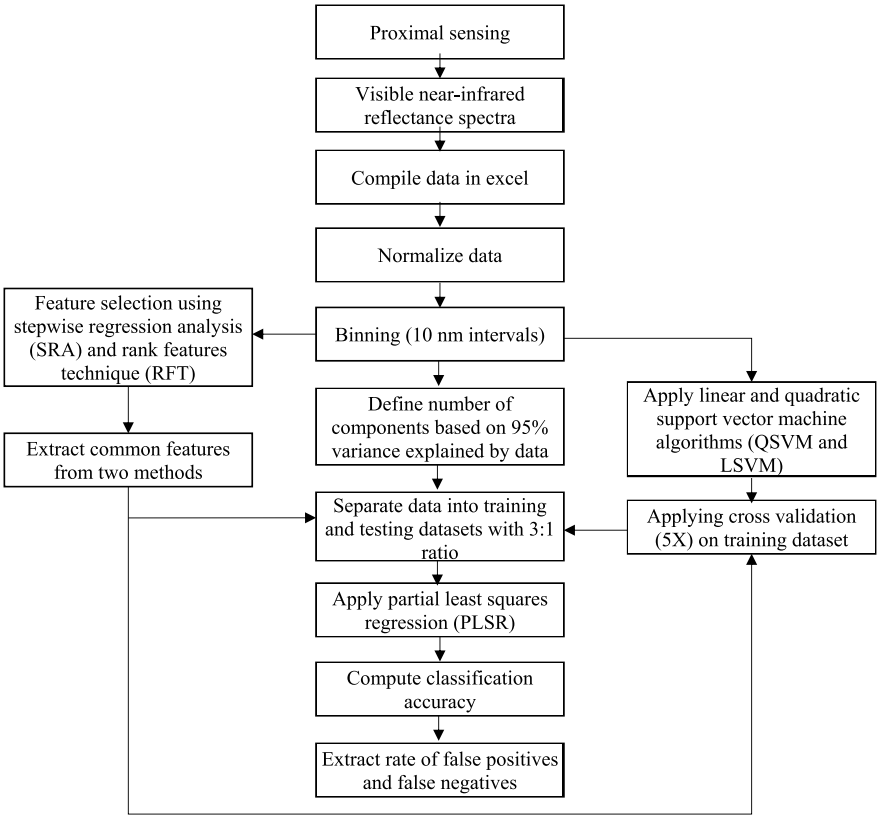

Fig. 2. Flowchart explaining processing steps of visible near-infrared (Vis-NIR) reflectance spectra.

Washington State University). In this study, the stomatal conductance measurements were compared to the same day visible-near infrared reflectance data of the treated trees.

2.3. Data collection

Vis-NIR reflectance data were collected using a spectroradiometer (SVC HR-1024i, Spectra Vista Corporation, NY, USA) with a working wavelength of 350–2500 nm. The resolution at 700, 1500 and 2100 nm, is ≤3.5, ≤9.5 and ≤6.5 nm, respectively. Three mature leaves exposed to sunlight were selected from different shoots in each tree, and data were captured using a leaf clip probe (LC-RP PRO, Spectra Vista Corporation, NY, USA). In total, 45 spectra from ABA-treated and untreated (control) tree leaves (total of 45 leaves) were collected. In addition to the proximal Vis-NIR spectral data, images from a modified multispectral digital imager (Canon ELPH110 HS, NJ, USA) and a thermal infrared imager (Tau 2 640, FLIR® Systems, OR, USA) were acquired. The imagers were mounted on an agricultural utility vehicle (John Deere Gator™ XUV590i, John Deere, IL, USA) connected to a retractable mast (FM50-25, Floatagraph Technologies, CA, USA). The distance between the imagers and trees was approximately 7 m. During data collection, the camera was always parallel to the ground surface, and images were acquired from the top of the tree canopies.

The three bands captured in the multispectral images were green (G), blue (B), and near infrared (NIR, 680–800 nm) with a resolution of 4608 × 3456. The thermal imager captured 8-bit images with 327,680 pixels and resolution of 640 × 512. The imaging sensors were connected to a triggering device and were manually triggered for simultaneous image acquisition. Images were stored in an on-board secure digital (SD) card and post-processed. The ground sampling distances for the multispectral imaging sensor was 2.5 mm and that of thermal imaging sensor was 8 mm. A white reflectance reference panel (Spectralon Reflectance Standard, Labsphere, North Sutton, NH) was used for radiometrically correcting the Vis-NIR reflectance spectra. The proximal data and images were collected 2 days after treatment (DAT) during the first ABA application (ABA-Application-1), and 1 day before treatment (DBT) and 1 and 3 DAT during the second ABA application (ABA-Application-2).

2.4. Data analysis

2.4.1. Vis-NIR spectral reflectance data

The data analysis was performed using Matlab® software, Statistics and Machine Learning toolboxes (Mathworks, Natick, MA). The Vis-NIR reflectance spectra were normalized and binned by averaging every 10 nm spectral interval (Sankaran et al., 2011) prior to further processing and analysis. Partial least square regression (PLSR), linear support vector machine (LSVM), and quadratic support vector machine (QSVM) algorithms were utilized for classification. PLSR is a multivariate analysis that is able to predict a set of dependent variables from a very large set of independent variables (i.e., predictors). This method is useful to predict the canopy status using Vis-NIR spectral signature as the predictor. The method includes partial least square analysis and multiple linear regression with combined features. PLSR extracts latent variables for prediction purposes (Abdi, 2010). The explained variance of 95% was used for selecting latent variables during PLSR analysis. For linear classification methods, SVM algorithms look for optimal separating hyperplanes between the classes. The classifier maximizes the margin between the support vector and the boundaries to optimize the algorithm. When data are not linearly separable, they are mapped to a higher dimensional space. In QSVM algorithms, data points are transported to a quadratic space and are separated by a plane. The classification algorithms were applied to assess the possibility of discriminating treated from untreated leaves. Each algorithm was applied three times on each dataset after randomization. The dataset was separated into training (for model development) and testing (for independent validation of the developed model) datasets with a ratio of 3:1 (Jarolmasjed et al., 2017). The average overall classification

accuracies, false positives (control classified as ABA-treated), and false negatives (ABA-treated classified as untreated) for each dataset are reported.

Highly dimensional data are computationally expensive and such data also introduce redundancy associated with correlated features in the spectrum (Pal and Foody, 2010). To reduce the data dimensionality, two feature selection methods, stepwise regression analysis (SRA) and rank features technique (RFT) were used. The bands that were selected by both methods were identified and validated using classification algorithms. Two additional bands selected by SRA were included and classification algorithms were assessed once more. Fig. 2 outlines the data processing steps used during feature selection and classification processes. The stomatal conductance prediction was performed using Vis-NIR reflectance spectra and the selected spectral features using PLSR.

In addition to multivariate analysis, several vegetation indices based on canopy greenness, photosynthesis, light use efficiency, nitrogen concentration, and canopy water content were estimated. Specific vegetative indices including normalized difference vegetation index (NDVI) (Rouse, 1974), enhanced vegetation index (EVI) (Huete et al., 2002), green normalized difference vegetation index (GNDVI) (Gitelson and Merzlyak, 1998), simple ratio (SR) (Birth and McVey, 1968), modified red edge normalized vegetation index (MRENDI) (Datt, 1999; Sims and Gamon, 2002), Vogelmann red edge index 1 (VREI1) (Vogelmann et al., 1993), Vogelmann red edge index 2 (VREI2) (Vogelmann et al., 1993), photochemical reflectance index (PRI) (Gamon et al., 1997; Peñuelas et al., 1995), structural independent pigment index (SIPI) (Penuelas et al., 1995), normalized difference nitrogen index (NDNI) (Fourty et al., 1996; Serrano et al., 2002), moisture stress index (MSI) (Ceccato et al., 2001; Hunt and Rock, 1989), normalized difference infrared index (NDII) (Hardisky et al., 1983), normalized difference water index (NDWI) (Gao, 1995; Jackson et al., 2004), normalized multi-band drought index (NMDI) (Wang et al., 2008; Wang and Qu, 2007), and water band index (WBI) (Peñuelas et al., 1993) were estimated. The purpose of extracting these features was to determine if any of the standard vegetation features can be used for assessing ABA effects on leaves and the overall tree. Statistical analysis was performed using R x64 (version 3.1.1, R Foundation for Statistical Computing, Vienna, Austria). Analysis of variance and 'student t-test' were used to compare the mean differences of vegetation indices.

2.4.2. Multispectral and thermal images

A representative multispectral image is shown in Fig. 3. In the multispectral camera, images were separated into individual band images, and the digital numbers were radiometrically corrected based on the reflectance from the reference panel. The goal of radiometric correction is to compensate for the changing incident light conditions during the imaging. Correction assists in obtaining absolute reflectance measurements from the images (Kelcey and Lucieer, 2012). Reference panel reflects 99% of the incident light (expected digital number = 255) in each of the spectral bands. If different, the digital numbers are corrected based on the correction factor calculated from the image digital number. Each pixel of the image is multiplied by the correction factor (ratio of 255/digital number of reference panel in the image). This correction normalizes the images for the changing sunlight conditions. Following this correction, GNDVI images were generated. The soil background and leaf shadows were eliminated with a combination of k-means clustering (Al Bashish et al., 2011) and thresholding methods (Bulanon et al., 2001). Individual trees then were segmented from the processed image, and the average GNDVI from each region of interest (tree) was extracted. The data were further analyzed statistically using R at 5% level of significance.

Thermal images were converted to comma separated value (CSV) files using ThermoViewer (2.0.2, Teax technology, Wilnsdorf, Germany). In thermal images, each pixel value represents the temperature in Celsius. Therefore, during the conversion to CSV format, the pixel temperature was preserved and recalled during image processing. In image processing algorithm, the soil background was removed by thresholding. The algorithm was able to automatically process the data for defined regions of interest. In preprocessed and corrected images, each tree was selected as a region of interest. A wide range of studies has used thermal imaging to assess the thermal properties of the canopies (Cohen et al., 2005; Fuentes et al., 2012; Gonzalez-Dugo et al., 2012; Grant et al., 2006; Jones, 2002). Thermal images are normalized using a crop water stress index (CWSI) to compensate the variability in the environmental parameters. This index that is extracted from thermal images is proportional to the stress level of crops (Berni et al., 2009). Thermal imaging is providing opportunities to sense the transpiration and stomatal conductance remotely with the help of CWSI. However, it is applicable only for a short span of time around solar noon and under the clear sky (DeJonge et al., 2015). It also requires some other measurements such as air temperature, lower and upper baseline that can be limited. In this study, images were normalized by the method described in Bellvert et al. (2014). In this method, mean, the minimum, and maximum temperature of each tree were extracted and recorded. Then, crop water stress index (CWSI) was extracted from the thermal images using the following equation.

$$CWSI = \frac{(T_c - T_a) - (T_{cmax} - T_a)}{(T_{cmin} - T_a) - (T_{cmax} - T_a)}$$

Where T_c represents the average canopy temperature in each region of interest of trees, and T_a is air temperature from a weather station in the orchard. T_{cmax} and T_{cmin} represent the maximum and minimum pixel temperature within each region of interest, respectively. The multispectral and thermal image processing protocol is summarized in Fig. 4.

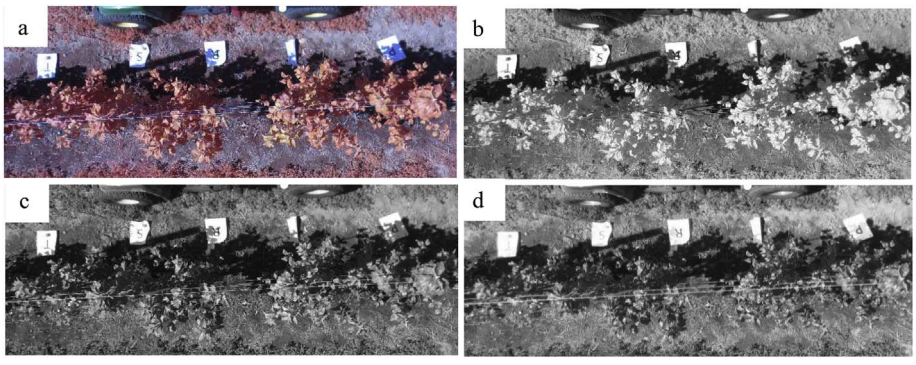

Fig. 3. The multispectral image (a) with near infrared (NIR) (b), green (c), and blue (d) bands. (For interpretation of the references to colour in this figure legend, the reader is referred to the Web version of this article.)

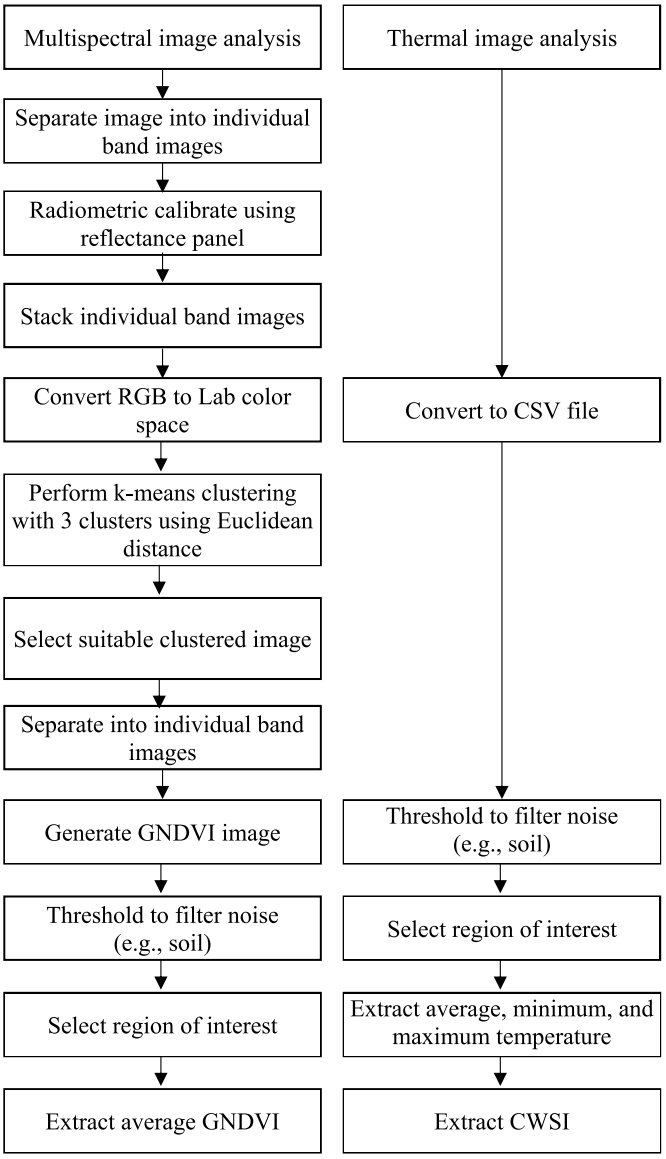

Fig. 4. Analysis flowchart of multispectral and thermal images acquired from the agricultural utility vehicle. GNDVI = green normalized difference vegetation index, CWSI = crop water stress index.

3. Results and discussion

3.1. Vis-NIR spectral reflectance data

Exogenous ABA applications induced stomatal closure in leaves and reduced leaf transpiration. Before Vis-NIR reflectance spectra analysis, the changes of the leaf stomatal conductance after the second treatment were analyzed. The mean stomatal conductance was greater in leaves from the untreated control compared to leaves from trees treated with exogenous ABA ($p < 0.05$). The p-value for data at 1 and 3 DAT after the ABA-Application-2 was < 0.001.

The Vis-NIR reflectance spectra from leaves were analyzed using PLSR, LSVM, and QSVM. The control and ABA-treated leaves were considered as two classes and the average overall classification accuracies are presented in Table 1. The classification accuracies in identifying the ABA-treated and control trees using three classification models were higher at 3 DAT after the ABA-Application-2, with average overall classification accuracies ranging from 80 to 85%. Overall, PLSR showed a better performance in the classification with the least false positive and false negative accuracies compared to SVM algorithms.

Table 1
Average overall classification accuracies, false positive, and false negative rates (± standard deviation) using different classification algorithms on the visible-near infrared reflectance spectra (350–2500 nm). DAT and DBT refer to days after treatment and day before treatment, respectively.

Model	Parameter	ABA-Application-1	ABA-Application-2		
		2 DAT	1 DBT	1 DAT	3 DAT
PLSR	Classification accuracy (%)	67 ± 7	68 ± 12	82 ± 5	85 ± 5
	False positive (%)	8 ± 3	11 ± 5	6 ± 5	3 ± 5
	False negative (%)	17 ± 5	18 ± 9	9 ± 9	3 ± 3
LSVM	Classification accuracy (%)	56 ± 9	52 ± 5	76 ± 5	80 ± 5
	False positive (%)	9 ± 8	26 ± 10	9 ± 0	17 ± 5
	False negative (%)	32 ± 12	23 ± 9	15 ± 5	12 ± 5
QSVM	Classification accuracy (%)	58 ± 19	55 ± 0	77 ± 5	85 ± 10
	False positive (%)	11 ± 15	30 ± 10	12 ± 3	9 ± 5
	False negative (%)	32 ± 5	15 ± 10	11 ± 7	9 ± 8

This classification approach supports the differences in the Vis-NIR spectral reflectance data between the control and ABA treatments. However, this difference was not observed at 1 DAT, especially after the ABA-Application-1. During the ABA-Application-2, 1 DAT also showed better classification accuracies that were only slightly lower than 3 DAT (76–82%).

SRA and RFT were applied to the dataset that showed the highest classification accuracy (3 DAT, ABA-Application-2, Table 1) to reduce 217 spectral features acquired from the processed raw data (after normalization and binning) to about 5 spectral features. The spectral features selected from these two models are summarized in Table 2. One set of three spectral features (960, 1140, 1150 nm; commonly selected spectral bands from two methods), and another set of five spectral features (580, 730, 960, 1140, 1150 nm; with the inclusion of green and red-edge spectral bands from SRA technique) were selected. In other studies, the wavelengths close to the included green and red-edge are suggested to be representative of plant responses to physiological stresses. Schlemmer et al. (2005) used first derivatives at 525–570 nm as well as red edge to measure physiological parameters in corn. Similarly Carter (1998) concluded that the reflectance near 550 and 700 nm is affected by physiological stress and chlorophyll content. The classification algorithms were then applied to the spectral data at 1 and 3 DAT after ABA-Application-2. Amongst all the datasets, the average classification accuracy at 3 DAT was the highest, but marginally lower than the entire Vis-NIR spectra (350–2500 nm, Table 3). The overall average classification accuracies of PLSR and LSVM was about 80%. The classification was more accurate with five spectral features (5-Bands) compared to three spectral features (3-Bands). There was no significant difference either between days after treatment or among the methods. However, the occurrence of false negative classifications was lower at 3 DAT.

During the PLSR-based prediction using Vis-NIR reflectance spectra (350–2500 nm), a strong regression coefficient between observed and

Table 2
Spectral features selected using stepwise regression analysis (SRA) and rank features technique (RFT) extraction techniques.

Feature selection technique	Selected spectral features (nm)
SRA	1140, 1250, 960, 340, 530, 580, 740, 730, 550, 1150
RFT	1140, 980, 1390, 1400, 970, 1150, 1880, 1380, 960, 1130

Table 3
Average overall classification accuracies, false positive, and negative rates (± standard deviation) using different classification algorithms on the selected spectral features using two feature extraction methods. 3-Bands include 960, 1140, and 1150 nm. 5-Bands include 580, 730, 960, 1140, and 1150 nm. DAT refers to days after treatment.

Algorithm	Parameters	3-Bands		5-Bands	
		1 DAT	3 DAT	1 DAT	3 DAT
PLSR	Classification accuracy (%)	68 ± 17	76 ± 9	73 ± 12	79 ± 9
	False positive (%)	18 ± 12	17 ± 9	17 ± 9	15 ± 10
	False negative (%)	14 ± 5	8 ± 5	11 ± 3	6 ± 3
LSVM	Classification accuracy (%)	69 ± 13	76 ± 7	65 ± 14	80 ± 5
	False positive (%)	20 ± 10	18 ± 8	27 ± 9	8 ± 3
	False negative (%)	11 ± 3	6 ± 3	8 ± 5	12 ± 7
QSVM	Classification accuracy (%)	64 ± 12	74 ± 7	70 ± 13	74 ± 12
	False positive (%)	26 ± 9	20 ± 7	23 ± 8	12 ± 7
	False negative (%)	11 ± 3	6 ± 3	8 ± 5	17 ± 13

predicted stomatal conductance was seen at both 1 DAT (R^2 = 0.98) and 3 DAT (R^2 = 0.96) as shown in Fig. 5. Root mean square error (*RMSE*) was 22.9 mmol/m^2.s for 1 DAT and the values were significantly correlated (r = 0.99, p < 0.001). Similarly, correlation for 3 DAT was significant (r = 0.98, p < 0.001) and RMSE was calculated as 31.1 mmol/m^2.s. In the case of using the PLSR model for post-feature selection, the regression coefficient between observed and predicted stomatal conductance decreased significantly. For 1 DAT (ABA-Application-2), the R^2 were 0.44 and 0.04 for 5-bands and 3-bands, respectively. Meanwhile, for 3 DAT, the observed R^2 were 0.17 for 5-bands and 0.11 for 3-bands datasets. These results indicated that 3-bands and 5-bands may not be sufficient for accurate stomatal conductance prediction, although differences between the ABA-treated and control trees can still be detected.

In addition to Vis-NIR spectra based classification, vegetation indices were computed to assess their potential in identifying differences in ABA-treated and control trees (Table 4). Amongst the evaluated indices, only PRI that is indicative of photosynthetic light-use efficiency showed significant differences between control and ABA-treated trees at 1 and 3 DAT after the ABA-Application-2 (Fig. 6). ABA controls stomatal conductance that influences photosynthesis rate (Astacio and Iersel, 2011). Studies indicate that photosynthetic radiation-use efficiency correlates with PRI (Barton and North, 2001; Gamon et al., 1997). Lower light-use efficiency in response to the closed stomata reduces the PRI. This could be the reason for observing treatment effects on PRI in this study, amongst evaluated vegetation indices.

3.2. Multispectral and thermal images

The GNDVI data were extracted from multispectral images with a region of interest on the tree leaves cluster from the top view. The results indicated that there were no significant differences in GNDVI and CWSI data extracted from control and ABA-treated trees, although differences in stomatal conductance were observed. This shows a major limitation in vegetation indices signifying they are not reliable indicators of short-term changes in plant health or performance including rapid changes in stomatal conductance. Visible ranges of the spectrum are representative of chlorophyll interactions with solar radiation. Meanwhile wavelength beyond 900 nm are influenced by changes in water content and dry matter (Haboudane et al., 2002). Ceccato et al. (2002) reported the limitations of normalized difference vegetation index in relation to vegetation water content. The information provided by vegetation greenness is not directly related to the water-related properties. Eitel et al. (2008) also reported the limitations of chlorophyll related indices because of their sensitivity to leaf area and coverage in response to soil moisture content.

Although a slightly higher average temperature in ABA-treated trees was observed as expected (lower stomatal conductance will induce stomatal closure and higher temperature), this difference was not significant (Fig. 7). O'Donoughue et al. (2011) reported a higher leaf temperature in plants treated with exogenous ABA. CWSI has also been used in water stress detection. The relationship between changes in plant canopy temperature corresponds to changes in crop water status (Bellvert et al., 2014). However, there are limitations associated with this method, specifically interferences of soil background temperatures that are also included in the canopy temperature measurement (Barnes et al., 2000). These limitations can increase variability and reduce the potential of vegetation indices in providing enough data to measure the physiological changes in leaves.

4. Conclusion

In this study, Vis-NIR spectral reflectance in the ranges of 350–2500 nm was used to detect the effect of exogenous ABA on apple trees. The result of PLSR on the Vis-NIR data from three days after ABA treatment showed the highest classification accuracy of 85%, with low false positive and false negative values compared to LSVM and QSVM analyses. The coefficient of determination for stomatal conductance prediction was as high as 0.96. Suitable spectral features were selected using RFT and SDA. While the classification accuracy was maintained at 80% with LSVM after reduction of features, the prediction accuracy decreased drastically. In addition to Vis-NIR data, multispectral and thermal images were captured from the trees. The CWSI data extracted from the thermal images, showed an increasing pattern with the reduction of stomatal conductance. However, GNDVI was not able to explain the effect of ABA on the leaves. These experiments provide important confirmations of a close relationship between direct

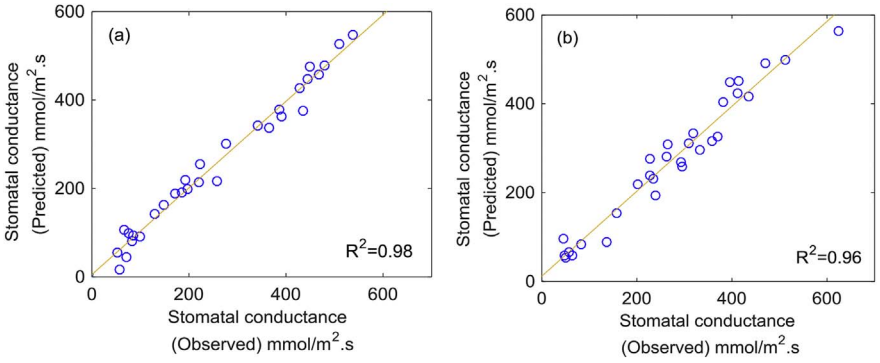

Fig. 5. The observed and predicted stomatal conductance at 1 day (a) and 3 days (b) after ABA-Application-2.

Table 4
Mean vegetation index (VI) data ± standard deviation of the control and ABA-treated leaves. The VIs evaluated are as follows: NDVI = normalized difference vegetation index, EVI = enhanced vegetation index, GNDVI = green normalized difference vegetation index, SR = simple ratio, MRENDI = modified red edge normalized vegetation index, VREI1 = Vogelmann red edge index 1, VREI2 = Vogelmann red edge index 2, PRI = photochemical reflectance index, SIPI = structural independent pigment index, NDNI = normalized difference nitrogen index, MSI = moisture stress index, NDII = difference infrared index, NDWI = normalized difference water index, NMDI = normalized multi-band drought index, WBI = water band index. DAT = days after treatment, DBT = days before treatment.

VI	Mean vegetation index data ± standard deviation							
	ABA-Application-1		ABA-Application-2					
	2 DAT		1 DBT		1 DAT		3 DAT	
	Control	Treated	Control	Treated	Control	Treated	Control	Treated
NDVI	0.89 ± 0.01	0.89 ± 0.02	0.86 ± 0.02	0.86 ± 0.02	0.86 ± 0.02	0.87 ± 0.02	0.86 ± 0.02	0.86 ± 0.02
EVI	0.12 ± 0.002	0.12 ± 0.002	0.12 ± 0.002	0.12 ± 0.001	0.12 ± 0.002	0.12 ± 0.002	0.12 ± 0.002	0.12 ± 0.002
GNDVI	0.75 ± 0.03	0.74 ± 0.05	0.71 ± 0.03	0.71 ± 0.05	0.71 ± 0.04	0.71 ± 0.05	0.70 ± 0.03	0.71 ± 0.05
SR	17.44 ± 2.29	17.14 ± 2.52	13.71 ± 1.91	13.59 ± 1.70	13.64 ± 1.76	14.08 ± 1.90	13.25 ± 1.73	13.14 ± 1.57
MRENDI	0.70 ± 0.05	0.68 ± 0.08	0.69 ± 0.05	0.69 ± 0.07	0.68 ± 0.06	0.68 ± 0.08	0.67 ± 0.05	0.68 ± 0.07
VREI1	1.67 ± 0.12	1.63 ± 0.15	1.64 ± 0.11	1.65 ± 0.13	1.63 ± 0.12	1.63 ± 0.14	1.60 ± 0.10	1.62 ± 0.13
VREI2	0.68 ± 0.08	0.65 ± 0.10	0.68 ± 0.09	0.69 ± 0.10	0.67 ± 0.09	0.67 ± 0.10	0.66 ± 0.08	0.68 ± 0.10
PRI	0.68 ± 0.03*	0.69 ± 0.04*	0.08 ± 0.02	0.07 ± 0.02	0.07 ± 0.01**	0.07 ± 0.02**	0.07 ± 0.01***	0.07 ± 0.02***
SIPI	0.89 ± 0.01	0.89 ± 0.01	0.86 ± 0.02	0.86 ± 0.02	0.86 ± 0.02	0.87 ± 0.02	0.86 ± 0.02	0.86 ± 0.02
NDNI	0.07 ± 0.003	0.07 ± 0.004	0.07 ± 0.003	0.07 ± 0.003	0.07 ± 0.003	0.07 ± 0.003	0.07 ± 0.004	0.07 ± 0.003
MSI	0.44 ± 0.04	0.43 ± 0.04	0.46 ± 0.04	0.46 ± 0.03	0.45 ± 0.03	0.45 ± 0.04	0.46 ± 0.04	0.46 ± 0.03
NDII	0.36 ± 0.03	0.36 ± 0.04	0.35 ± 0.03	0.35 ± 0.03	0.36 ± 0.03	0.36 ± 0.03	0.35 ± 0.04	0.36 ± 0.03
NDWI	0.07 ± 0.01	0.07 ± 0.01	0.07 ± 0.01	0.07 ± 0.01	0.07 ± 0.01	0.07 ± 0.01	0.07 ± 0.01	0.07 ± 0.01
NMDI	0.52 ± 0.02	0.53 ± 0.02	0.53 ± 0.02	0.53 ± 0.02	0.53 ± 0.02	0.53 ± 0.02	0.53 ± 0.02	0.53 ± 0.02
WBI	0.95 ± 0.01	0.95 ± 0.01	0.96 ± 0.01	0.95 ± 0.01	0.95 ± 0.01	0.96 ± 0.01	0.96 ± 0.01	0.96 ± 0.01

*p = 0.02, **p = 0.05; ***p = 0.03.

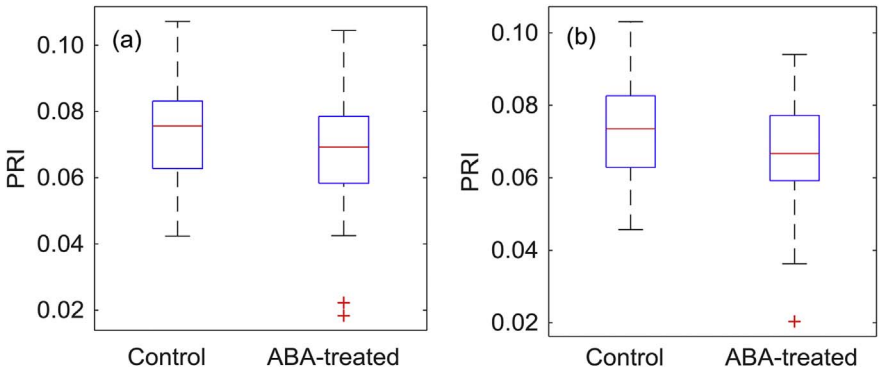

Fig. 6. Boxplot showing photochemical reflectance index (PRI) at 1 (a) and 3 (b) days after treatment. The box plot displays the minimum, median, maximum (box boundaries and center line); first and third quartile (top and bottom of whiskers); and outlier values (marked as +).

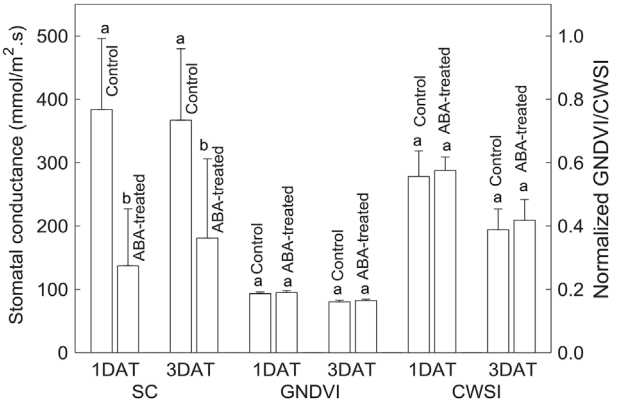

Fig. 7. Stomatal conductance (SC) and green normalized difference vegetation index (GNDVI) per crop water stress index (CWSI) values at 1 and 3 DAT after the ABA-Application-2. Bars indicate the standard deviation of the means. A *t*-test was conducted (α = 0.05) for each treatment, the same letter within each dataset shows treatments that were not significantly different.

physiological measurements of stomatal conductance and modeled estimations from Vis-NIR hyperspectral reflectance data. Proximal sensing of stomatal conductance using Vis-NIR reflectance spectra can be used to measure the plant response from exogenous ABA applications.

Acknowledgement

We like to extend our gratitude to Carlos Zúñiga Espinoza, Katie Mullin, Michelle Reid, and Jordan Briggs for their help during this study. This work was funded, in part, by the Washington Tree Fruit Research Commission (AP-15-101) and USDA National Institute for Food and Agriculture, Hatch Project, 1002864 (WNP00821).

References

Aasamaa, K., Sõber, A., 2011. Stomatal sensitivities to changes in leaf water potential, air humidity, CO2 concentration and light intensity, and the effect of abscisic acid on the sensitivities in six temperate deciduous tree species. Environ. Exp. Bot. 71, 72–78. https://doi.org/10.1016/j.envexpbot.2010.10.013.

Abdi, H., 2010. Partial least squares regression and projection on latent structure regression (PLS Regression). Wiley Interdiscipl. Rev. Comput. Stat. 2, 97–106. https://doi.org/10.1002/wics.51.

AgWeatherNet at Washington State University, n.d. Available online: http://weather.wsu.

edu/. (Accessed 1 September 2017).
Al Bashish, D., Braik, M., Bani-Ahmad, S., 2011. Detection and classification of leaf diseases using K-means-based segmentation and neural-network-based classification. Inf. Technol. J. 10, 267–275.
Araus, J.L., Cairns, J.E., 2014. Field high-throughput phenotyping: the new crop breeding frontier. Trends Plant Sci. 19, 52–61. https://doi.org/10.1016/j.tplants.2013.09.008.
Astacio, M.G., Iersel, M.W. van, 2011. Determining the effects of abscisic acid drenches on evapotranspiration and leaf gas exchange of tomato. HortScience 46, 1512–1517.
Barnes, E., Clarke, T.R., Richards, S.E., Colaizzi, P., Haberland, J., Kostrzewski, M., Waller, P., Choi, C., Riley, E., Thompson, T., 2000. Coincident Detection of Crop Water Stress, Nitrogen Status, and Canopy Density Using Ground Based Multispectral Data.
Barton, C.V.M., North, P.R.J., 2001. Remote sensing of canopy light use efficiency using the photochemical reflectance index: model and sensitivity analysis. Remote Sens. Environ. 78, 264–273. https://doi.org/10.1016/S0034-4257(01)00224-3.
Bellvert, J., Zarco-Tejada, P.J., Girona, J., Fereres, E., 2014. Mapping crop water stress index in a 'Pinot-noir' vineyard: comparing ground measurements with thermal remote sensing imagery from an unmanned aerial vehicle. Precis. Agric. 15, 361–376. https://doi.org/10.1007/s11119-013-9334-5.
Berkowitz, G.A., Rabin, J., 1988. Antitranspirant associated abscisic acid effects on the water relations and yield of transplanted bell peppers. Plant Physiol. 86, 329–331. https://doi.org/10.1104/pp.86.2.329.
Berni, J.A.J., Zarco-Tejada, P.J., Sepulcre-Cantó, G., Fereres, E., Villalobos, F., 2009. Mapping canopy conductance and CWSI in olive orchards using high resolution thermal remote sensing imagery. Remote Sens. Environ. 113, 2380–2388. https://doi.org/10.1016/j.rse.2009.06.018.
Birth, G.S., McVey, G.R., 1968. Measuring the color of growing turf with a reflectance spectrophotometer. Agron. J. 60, 640–643. https://doi.org/10.2134/agronj1968.00021962006000060016x.
Bulanon, D.M., Kataoka, T., Zhang, S., Ota, Y., Hiroma, T., 2001. Optimal Thresholding for the Automatic Recognition of Apple Fruits. American Society of Agricultural and Biological Engineers. https://doi.org/10.13031/2013.3672.
Calderón, R., Navas-Cortés, J.A., Lucena, C., Zarco-Tejada, P.J., 2013. High-resolution airborne hyperspectral and thermal imagery for early detection of Verticillium wilt of olive using fluorescence, temperature and narrow-band spectral indices. Remote Sens. Environ. 139, 231–245. https://doi.org/10.1016/j.rse.2013.07.031.
Calderón, R., Montes-Borrego, M., Landa, B.B., Navas-Cortés, J.A., Zarco-Tejada, P.J., 2014. Detection of downy mildew of opium poppy using high-resolution multispectral and thermal imagery acquired with an unmanned aerial vehicle. Precis. Agric. 15, 639–661. https://doi.org/10.1007/s11119-014-9360-y.
Carter, G.A., 1998. Reflectance wavebands and indices for remote estimation of photosynthesis and stomatal conductance in pine canopies. Remote Sens. Environ. 63, 61–72.
Ceccato, P., Flasse, S., Tarantola, S., Jacquemoud, S., Grégoire, J.-M., 2001. Detecting vegetation leaf water content using reflectance in the optical domain. Remote Sens. Environ. 77, 22–33. https://doi.org/10.1016/S0034-4257(01)00191-2.
Ceccato, P., Flasse, S., Grégoire, J.-M., 2002. Designing a spectral index to estimate vegetation water content from remote sensing data: Part 2. Validation and applications. Remote Sens. Environ. 82, 198–207. https://doi.org/10.1016/S0034-4257(02)00036-6.
Chaerle, L., Saibo, N., Van Der Straeten, D., 2005. Tuning the pores: towards engineering plants for improved water use efficiency. Trends Biotechnol. 23, 308–315. https://doi.org/10.1016/j.tibtech.2005.04.005.
Coggins Jr., C.W., Lovatt, C.J., 2014. Plant growth regulators. Citrus Prod. Manag. 3539, 215.
Cohen, Y., Alchanatis, V., Meron, M., Saranga, Y., Tsipris, J., 2005. Estimation of leaf water potential by thermal imagery and spatial analysis*. J. Exp. Bot. 56, 1843–1852. https://doi.org/10.1093/jxb/eri174.
Correia, M.J., Pereira, J.S., Chaves, M.M., Rodrigues, M.L., Pacheco, C.A., 1995. ABA xylem concentrations determine maximum daily leaf conductance of field-grown Vitis vinifera L. plants. Plant Cell Environ. 18, 511–521. https://doi.org/10.1111/j.1365-3040.1995.tb00551.x.
Datt, B., 1999. A new reflectance index for remote sensing of chlorophyll content in higher plants: tests using Eucalyptus leaves. J. Plant Physiol. 154, 30–36. https://doi.org/10.1016/S0176-1617(99)80314-9.
DeJonge, K.C., Taghvaeian, S., Trout, T.J., Comas, L.H., 2015. Comparison of canopy temperature-based water stress indices for maize. Agric. Water Manag. 156, 51–62. https://doi.org/10.1016/j.agwat.2015.03.023.
Eitel, J.U.H., Long, D.S., Gessler, P.E., Hunt, E.R., 2008. Combined spectral index to improve ground-based estimates of nitrogen status in dryland wheat. Agron. J. 100, 1694–1702. https://doi.org/10.2134/agronj2007.0362.
Espinoza, C.Z., Khot, L.R., Sankaran, S., Jacoby, P.W., 2017. High resolution multispectral and thermal remote sensing-based water stress assessment in subsurface irrigated grapevines. Rem. Sens. 9 (961). https://doi.org/10.3390/rs9090961.
Falchi, R., D'Agostin, E., Mattiello, A., Coronica, L., Spinelli, F., Costa, G., Vizzotto, G., 2017. ABA regulation of calcium-related genes and bitter pit in apple. Postharvest Biol. Technol. 132, 1–6. https://doi.org/10.1016/j.postharvbio.2017.05.017.
Fourty, T., Baret, F., Jacquemoud, S., Schmuck, G., Verdebout, J., 1996. Leaf optical properties with explicit description of its biochemical composition: direct and inverse problems. Remote Sens. Environ. 56, 104–117. https://doi.org/10.1016/0034-4257(95)00234-0.
Freitas, D., Tonetto, S., Shackel, K.A., Mitcham, E.J., 2011. Abscisic acid triggers whole-plant and fruit-specific mechanisms to increase fruit calcium uptake and prevent blossom end rot development in tomato fruit. J. Exp. Bot. 62, 2645–2656. https://doi.org/10.1093/jxb/erq430.
Fuentes, S., De Bei, R., Pech, J., Tyerman, S., 2012. Computational water stress indices obtained from thermal image analysis of grapevine canopies. Irrig. Sci. 30, 523–536. https://doi.org/10.1007/s00271-012-0375-8.
Gamon, J.A., Serrano, L., Surfus, J.S., 1997. The photochemical reflectance index: an optical indicator of photosynthetic radiation use efficiency across species, functional types, and nutrient levels. Oecologia 112, 492–501. https://doi.org/10.1007/s004420050337.
Gao, B.C., 1995. Normalized difference water index for remote sensing of vegetation liquid water from space [2480-19]. In: Proceedings-SPIE the International Society for Optical Engineering, 225.
García-Mata, C., Lamattina, L., 2003. Abscisic acid, nitric oxide and stomatal closure – is nitrate reductase one of the missing links? Trends Plant Sci. 8, 20–26. https://doi.org/10.1016/S1360-1385(02)00009-2.
Gitelson, A.A., Merzlyak, M.N., 1998. Remote sensing of chlorophyll concentration in higher plant leaves. Synergistic Use of Multisensor Data for Land Processes. Adv. Space Res. 22, 689–692. https://doi.org/10.1016/S0273-1177(97)01133-2.
Gomez-Candon, D., Labbé, S., Virlet, N., Jolivot, A., Regnard, J.-L., 2014. High resolution thermal and multispectral UAV imagery for precision assessment of apple tree response to water stress. In: 2. International Conference on Robotics and Associated High-technologies and Equipment for Agriculture and Forestry RHEA. PGM, Madrid, Spain p. np.
Gonzalez-Dugo, V., Zarco-Tejada, P., Berni, J.A.J., Suárez, L., Goldhamer, D., Fereres, E., 2012. Almond tree canopy temperature reveals intra-crown variability that is water stress-dependent. Agric. For. Meteorol. 154–155, 156–165. https://doi.org/10.1016/j.agrformet.2011.11.004.
Grant, O.M., Tronina, L., Jones, H.G., Chaves, M.M., 2006. Exploring thermal imaging variables for the detection of stress responses in grapevine under different irrigation regimes. J. Exp. Bot. 58, 815–825. https://doi.org/10.1093/jxb/erl153.
Haboudane, D., Miller, J.R., Tremblay, N., Zarco-Tejada, P.J., Dextraze, L., 2002. Integrated narrow-band vegetation indices for prediction of crop chlorophyll content for application to precision agriculture. Remote Sens. Environ. 81, 416–426. https://doi.org/10.1016/S0034-4257(02)00018-4.
Hardisky, M.A., Klemas, V., Smart, R.M., 1983. The influence of soil salinity, growth form, and leaf moisture on the spectral radiance of Spartina alterniflora canopies. Eng. Rem. Sens. 49, 77–83.
Hilhorst, H.W.M., Karssen, C.M., 1992. Seed dormancy and germination: the role of abscisic acid and gibberellins and the importance of hormone mutants. Plant Growth Regul. 11, 225–238. https://doi.org/10.1007/BF00024561.
Ho, L.C., White, P.J., 2005. A cellular hypothesis for the induction of blossom-end rot in tomato fruit. Ann. Bot. 95, 571–581. https://doi.org/10.1093/aob/mci065.
Huete, A., Didan, K., Miura, T., Rodriguez, E.P., Gao, X., Ferreira, L.G., 2002. Overview of the radiometric and biophysical performance of the MODIS vegetation indices. The Moderate Resolution Imaging Spectroradiometer (MODIS): a new generation of Land Surface Monitoring. Remote Sens. Environ. 83, 195–213. https://doi.org/10.1016/S0034-4257(02)00096-2.
Hunt, E.R., Rock, B.N., 1989. Detection of changes in leaf water content using Near- and Middle-Infrared reflectances. Remote Sens. Environ. 30, 43–54. https://doi.org/10.1016/0034-4257(89)90046-1.
Jackson, T.J., Chen, D., Cosh, M., Li, F., Anderson, M., Walthall, C., Doriaswamy, P., Hunt, E.R., 2004. Vegetation water content mapping using Landsat data derived normalized difference water index for corn and soybeans. 2002 Soil Moisture Experiment (SMEX02). Remote Sens. Environ. 92, 475–482. https://doi.org/10.1016/j.rse.2003.10.021.
Jarolmasjed, S., Espinoza, C.Z., Sankaran, S., 2017. Near infrared spectroscopy to predict bitter pit development in different varieties of apples. J. Food Meas. Charact. 11, 987–993. https://doi.org/10.1007/s11694-017-9473-x.
Jones, H.G., 2002. Use of infrared thermography for monitoring stomatal closure in the field: application to grapevine. J. Exp. Bot. 53, 2249–2260. https://doi.org/10.1093/jxb/erf083.
Kelcey, J., Lucieer, A., 2012. Sensor correction and radiometric calibration of a 6-band multispectral imaging sensor for UAV remote sensing. In: The 12th Congress of the International Society for Photogrammetry and Remote Sensing, pp. 393–398.
Kobashi, K., Gemma, H., Iwahori, S., 1999. Sugar accumulation in peach fruit as affected by abscisic acid (ABA) treatment in relation to some sugar metabolizing enzymes. J. Jpn. Soc. Hortic. Sci. 68, 465–470. https://doi.org/10.2503/jjshs.68.465.
McArtney, S.J., Abrams, S.R., Woolard, D.D., Petracek, P.D., 2014. Effects of S-abscisic acid and (+)-8′-acetylene abscisic acid on fruit set and stomatal conductance in apple. HortScience 49, 763–768.
Montanaro, G., Dichio, B., Xiloyannis, C., 2010. Significance of fruit transpiration on calcium nutrition in developing apricot fruit. J. Plant Nutr. Soil Sci. 173, 618–622. https://doi.org/10.1002/jpln.200900376.
Montanaro, G., Dichio, B., Xiloyannis, C., Lang, A., 2012. Fruit transpiration in kiwifruit: environmental drivers and predictive model. AoB Plants 2012. https://doi.org/10.1093/aobpla/pls036.
Naidu, R.A., Perry, E.M., Pierce, F.J., Mekuria, T., 2009. The potential of spectral reflectance technique for the detection of Grapevine leafroll-associated virus-3 in two red-berried wine grape cultivars. Comput. Electron. Agric. 66, 38–45. https://doi.org/10.1016/j.compag.2008.11.007.
O'Donoughue, A.E., Bartuska, C.A., Barrett, J.E., 2011. S-Abscisic acid effects on evapotranspiration and leaf burn in Salvia farinacea. In: Int. Symp. Adv. Technol. Manag. Sustain. Greenh. Ecosyst. Greensys Greensys 2011, pp. 287–293.
Osakabe, Y., Osakabe, K., Shinozaki, K., Tran, L.-S.P., 2014. Response of plants to water stress. Front. Plant Sci. 5. https://doi.org/10.3389/fpls.2014.00086.
Pal, M., Foody, G.M., 2010. Feature selection for classification of hyperspectral data by SVM. IEEE Trans. Geosci. Rem. Sens. 48, 2297–2307. https://doi.org/10.1109/TGRS.2009.2039484.
Peñuelas, J., Filella, I., Biel, C., Serrano, L., Savé, R., 1993. The reflectance at the 950–970

nm region as an indicator of plant water status. Int. J. Rem. Sens. 14, 1887–1905. https://doi.org/10.1080/01431169308954010.

Peñuelas, J., Filella, I., Gamon, J.A., 1995. Assessment of photosynthetic radiation-use efficiency with spectral reflectance. New Phytol. 131, 291–296. https://doi.org/10.1111/j.1469-8137.1995.tb03064.x.

Penuelas, J., Frederic, B., Filella, I., 1995. Semi-empirical Indices to Assess Carotenoids/Chlorophyll-a Ratio from Leaf Spectral Reflectance.

Rouse, J.W., 1974. Monitoring Vegetation Systems in the Great Plains with ERTS.

Sankaran, S., Mishra, A., Maja, J.M., Ehsani, R., 2011. Visible-near infrared spectroscopy for detection of Huanglongbing in citrus orchards. Comput. Electron. Agric. 77, 127–134. https://doi.org/10.1016/j.compag.2011.03.004.

Schlemmer, M.R., Francis, D.D., Shanahan, J.F., Schepers, J.S., 2005. Remotely measuring chlorophyll content in corn leaves with differing nitrogen levels and relative water content. Agron. J. 97, 106–112.

Serrano, L., Peñuelas, J., Ustin, S.L., 2002. Remote sensing of nitrogen and lignin in Mediterranean vegetation from AVIRIS data: decomposing biochemical from structural signals. Remote Sens. Environ. 81, 355–364. https://doi.org/10.1016/S0034-4257(02)00011-1.

Shackel, K.A., Ahmadi, H., Biasi, W., Buchner, R., Goldhamer, D., Gurusinghe, S., Hasey, J., Kester, D., Krueger, B., Lampinen, B., McGourty, G., Micke, W., Mitcham, E., Olson, B., Pelletrau, K., Philips, H., Ramos, D., Schwankl, L., Sibbett, S., Snyder, R., Southwick, S., Stevenson, M., Thorpe, M., Weinbaum, S., Yeager, J., 1997. Plant water status as an index of irrigation need in deciduous fruit trees. HortTechnology 7, 23–29.

Shinozaki, K., Yamaguchi-Shinozaki, K., 2007. Gene networks involved in drought stress response and tolerance. J. Exp. Bot. 58, 221–227. https://doi.org/10.1093/jxb/erl164.

Sims, D.A., Gamon, J.A., 2002. Relationships between leaf pigment content and spectral reflectance across a wide range of species, leaf structures and developmental stages. Remote Sens. Environ. 81, 337–354. https://doi.org/10.1016/S0034-4257(02)00010-X.

Vogelmann, J.E., Rock, B.N., Moss, D.M., 1993. Red edge spectral measurements from sugar maple leaves. Int. J. Rem. Sens. 14, 1563–1575. https://doi.org/10.1080/01431169308953986.

Wang, L., Qu, J.J., 2007. NMDI: a normalized multi-band drought index for monitoring soil and vegetation moisture with satellite remote sensing. Geophys. Res. Lett. 34, L20405. https://doi.org/10.1029/2007GL031021.

Wang, L., Qu, J.J., Hao, X., 2008. Forest fire detection using the normalized multi-band drought index (NMDI) with satellite measurements. Agric. For. Meteorol. 148, 1767–1776. https://doi.org/10.1016/j.agrformet.2008.06.005.

Zarco-Tejada, P.J., González-Dugo, V., Berni, J.A.J., 2012. Fluorescence, temperature and narrow-band indices acquired from a UAV platform for water stress detection using a micro-hyperspectral imager and a thermal camera. Remote Sens. Environ. 117, 322–337. https://doi.org/10.1016/j.rse.2011.10.007.